ACS APPLIED NANO MATERIALS

Article

Cite This: *ACS Appl. Nano Mater.* 2019, 2, 1223−1231

www.acsanm.org

Phase Behavior of *cis*−*trans* Mixtures of Double-Decker Shaped Silsesquioxanes for Processability Enhancement

David F. Vogelsang,[†] Jonathan E. Dannatt,[‡] Beth W. Schoen,[†] Robert E. Maleczka, Jr.,*[‡] and Andre Lee*[†]

[†]Department of Chemical Engineering and Materials Science, Michigan State University, 428 South Shaw Lane, East Lansing, Michigan 48824-1226, United States

[‡]Department of Chemistry, Michigan State University, 578 South Shaw Lane, East Lansing, Michigan 48824-1322, United States

Supporting Information

ABSTRACT: Closed double-decker shaped silsesquioxanes (DDSQ-$(Ph)_8$-2((Me)(R))) with R as phenyl, *para*-phenylamine, and *para*-phenylethynyl phenyl were synthesized. Isolation of nearly pure *trans* and *cis* isomers was obtained by fractional recrystallization. Crystallographic and thermal characteristics of these isolated isomers were obtained by X-ray diffraction of a single crystal and differential scanning calorimetry (DSC). It was observed that melting temperature increases as the size of the R group decreases from *para*-phenylethynyl phenyl to phenyl and the magnitude of the entropy difference at melting increases as the size of the R group increases. Isolated isomers were then mixed to different *cis*-to-*trans* ratios, and their thermal characteristics investigated by DSC. The upper portion of the phase diagram was constructed for these DDSQ compounds using results from DSC traces. Interestingly, *cis* and *trans* isomers of these DDSQ compounds form a binary eutectic. Experimentally observed eutectic composition and temperature were found to be close to the calculated values based on the ideal eutectic mixing rule. These data allow users to broaden the thermal processability window by reducing the system melting temperature without affecting the reaction onset temperature of the functional groups.

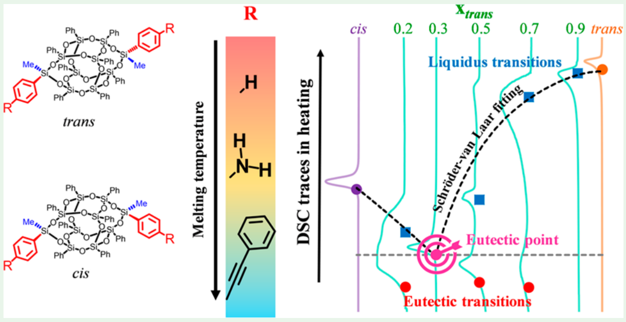

KEYWORDS: *double-decker shaped silsesquioxanes, melting temperature suppression, binary cis and trans eutectic composition, phase diagram*

■ INTRODUCTION

Functionalized double-decker shaped silsesquioxane (DDSQ-2(R_1R_2)) and corner capped cubic shaped silsesquioxanes (POSS-R_1) (Figure 1) are cage-like silsesquioxanes with a dimensionally well-defined inorganic core, inert organic groups around the core which provides compatibility with the surround organic matter of interest, and exact specified reactive organic sites.[1,2] These structures have become model compounds to investigate effects of nanostructured inorganic additives on polymer properties.[3−7] Applications of both DDSQ-2(R_1R_2) and POSS-R_1 nanostructures have been explored extensively.[1,3−5,8−30] When used in organic polymers, the hybrid characteristics provide enhanced oxidation temperature, improved hydrophobicity, and low dielectric constant.[10−14,19,29,31−36] Recent research extended the use of DDSQ-2(R_1R_2) and POSS-R_1 as supports to reduce the amount of packed bed required in heterogeneous catalysts.[5,10,37−40] Other applications for POSS-R_1 include improved ionic liquid performance and its thermal stability,[34,41−43] microstructure modifier to improve mechanical performance of metallic alloys,[25] superhydrophobicity in coatings,[27,44−46] monomer for increased thermal and mechanical performance of thermosetting polymers,[47−50] and use in pharmaceutical applications.[45,51−54]

Incorporation of POSS-R_1 or DDSQ-2(R_1R_2) without the use of solvents is an environmentally friendly method to integrate these cage-like silsesquioxanes into organic polymers and has been achieved by melting the nanostructures.[28,32,55,56]

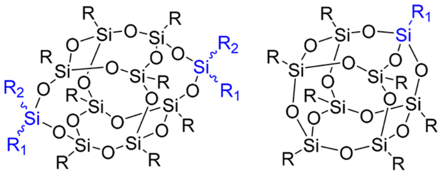
cis/trans-DDSQ-2(R_1R_2)   POSS-R_1

Figure 1. Structures of *cis*/*trans*-DDSQ-2(R_1R_2) and POSS-R_1 where R designations are inert organic moieties and R_1 and R_2 are active functional groups.

Received: November 21, 2018
Accepted: February 5, 2019
Published: February 5, 2019

DOI: 10.1021/acsanm.8b02114

In our prior work on POSS-(phenylethynylphthalimide) where the surrounding R moieties were phenyl or isobutyl, it was observed that heptaphenyl POSS-(phenylethynylphthalimide) did not melt; however, the isobutyl system could be melt-processed with organic oligomeric phenylethynylphthalimide to form thermosets.[32] Interestingly, it was found that octaphenyl DDSQ-2((phenylethynylphthalimide)(methyl)), which is structurally similar to heptaphenyl POSS-(phenylethynylphthalimide), resulted in a material that exhibited melt characteristics.[32,57] It was hypothesized that melting of DDSQ-2(R_1R_2) was caused by higher entropy as compared to POSS-R_1 because the as-synthesized DDSQ-2(R_1R_2) products contain *cis* and *trans* isomers about the inorganic core as shown in Scheme 1.[7,8,55,58−64]

Scheme 1. Condensation of 1 with 2 equiv of Organodichlorosilanes

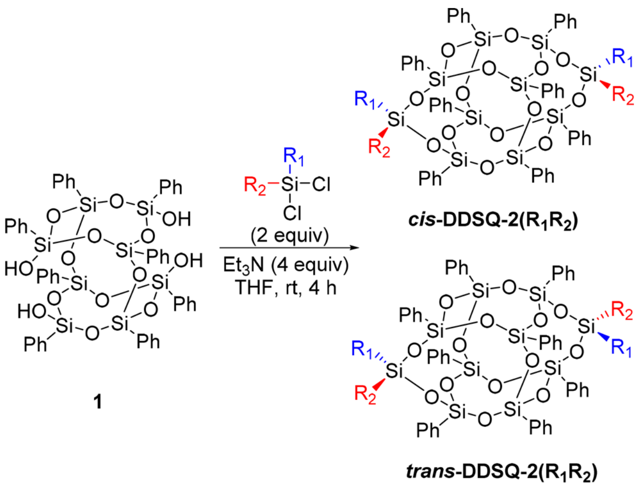

Separation of *cis* and *trans* DDSQ-2(R_1R_2) isomers using fractional crystallization (FC) and/or liquid chromatography (LC) has been achieved,[8,62] and it has been demonstrated that polymers synthesized from mostly *cis* isomers exhibit different thermal characteristics compared with the same polymer made with mostly *trans* isomers.[8] In this work we investigate the effect of bulkiness of an aryl group in the R_1 position in DDSQ-2((methyl)(R_1)) on the melting temperature of the *cis* or *trans* isomers. In addition, this work focused on a more systematic understanding of the melting behavior of DDSQ compounds with varying *cis* to *trans* ratios. Results from the differential scanning calorimetry (DSC) were used to construct the upper portion of the *cis*−*trans* binary phase diagram. The resulting binary phase diagram can be used to tailor a specified *cis* to *trans* ratio for optimizing the condition needed for melt mixing with organic polymers.

■ MATERIALS AND METHODS

All commercially available chemicals were used as received unless otherwise indicated. $(C_6H_5)_8Si_8O_{10}(OH)_4$ 5,11,14,17-tetra(hydro)-octaphenyltetracyclo[7.3.3.-$3^{3,7}$]octasilsesquioxane (DDSQ-$(Ph)_8(OH)_4$) **1** was purchased from Hybrid Plastics. Methyltrichlorosilane, 4-[bis(trimethylsilyl)amino]phenyl(bromo)magnesium, 4-bromoiodobenzene, phenylacetylene, phenylmethyldichlorosilane, Pd$(PPh_3)_2Cl_2$, CuI, activated magnesium turnings, $CDCl_3$ with 1% TMS, dichloromethane (DCM), hexanes, ethyl acetate, and THF were all purchased from commercial sources and used directly unless otherwise specified. THF was refluxed over sodium/benzophenone ketyl and distilled.

Synthesis of Dichloro(methyl)(4-(phenylamine(bis(trimethylsilyl))))silane. Under an N_2 atmosphere, a solution of 0.5 M 4-[bis(trimethylsilyl)amino]phenyl(bromo)magnesium in THF (30 mL, 15 mmol) was injected dropwise into a flask containing a solution of freshly distilled THF (10 mL) and 18 mmol of methyltrichlorosilane (1.2 equiv, 2.11 mL) that was cooled by an ice bath (Scheme 2). This mixture was allowed to warm to room temperature and then stir for 24 h after which a clear yellow-pale solution was observed. At the end of the reaction, the excess THF and $MeSiCl_3$ were removed by distillation under N_2 in an oil bath at 90 °C. The product was then distilled at 120 °C under 0.1 mmHg vacuum, producing a clear yellow liquid (3.95 g, 11.26 mmol, 75% yield). The spectra match previously reported data.[58,62] ^{1}H NMR (500 MHz, $CDCl_3$) δ: 7.58 (m, 2H), 7.01 (m, 2H), 1.02 (s, 3H, CH_3), 0.10 (s, 18H, TMS). ^{29}Si NMR (99 MHz, $CDCl_3$) δ 18.89 (1Si), 5.12 (2Si).

Scheme 2. Synthesis of Dichloro(methyl)(4-(phenylamine(bis(trimethylsilyl))))silane

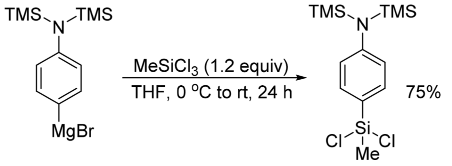

Synthesis of 1-Bromo-4-(phenylethynyl)benzene. This procedure was adapted from previous literature and described in Scheme 3.[61,64] To a 500 mL round-bottom flask were added 4-bromoiodobenzene (100 g, 353 mmol, 1 equiv), Pd$(PPh_3)_2Cl_2$ (0.2481 g, 0.353 mmol, 0.1 mol %), CuI (0.0673 g, 0.353 mmol, 0.1 mol %), and a stir bar. The flask was sealed with a rubber septum and flushed with nitrogen before 300 mL of freshly distilled THF was added. Triethylamine (54.3 mL, 0.389 mol, 1.1 equiv) was distilled over CaH_2 and added to the reaction mixture. Finally, phenylacetylene (42.7 mL, 0.389 mol, 1.1 equiv) was added dropwise to the reaction mixture. The reaction solution eventually turned a brown color and formed a white precipitate. The white precipitate is likely Et_3NI. The reaction was allowed to stir for 12 h at room temperature. At the end of the reaction, the solvent was removed, and the resulting solid was extracted with DCM/H_2O. The organic layer was dried with magnesium sulfate and concentrated and the resultant solid was then purified by silica column chromatography (hexanes) to afford 87.25 g of a white flaky solid (96% yield, mp 82−85 °C) with NMR data matching those previously reported in the literature.[65] ^{1}H NMR (500 MHz, $CDCl_3$) δ 7.57−7.53 (m, 2H), 7.52−7.48 (m, 2H), 7.44−7.39 (m, 2H), 7.39−7.35 (m, 3H). ^{13}C NMR (126 MHz, $CDCl_3$) δ 133.04, 132.52, 131.62 (d, J = 2.3 Hz), 128.53, 128.42, 122.92, 122.49, 122.25, 90.53, 88.34.

Scheme 3. Synthesis of 1-Bromo-4-(phenylethynyl)benzene

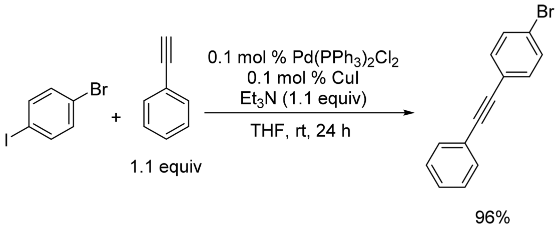

Synthesis of Dichloro(methyl)(4-(phenylethynyl)phenyl)silane. Following Scheme 4, to a 250 mL round-bottom flask were added Mg^0 turnings (2.08 g, 0.085 mol, 1.1 equiv) and a stir bar. The Mg^0 turnings were stirred under vacuum for 2 h after which the contents were put under an N_2 atmosphere. 1-Bromo-4-(phenylethynyl)benzene (20 g, 0.077 mol, 1 equiv) was dissolved in 80 mL of freshly distilled THF and injected into the flask containing

Scheme 4. Synthesis of Dichloro(methyl)(4-(phenylethynyl)phenyl)silane

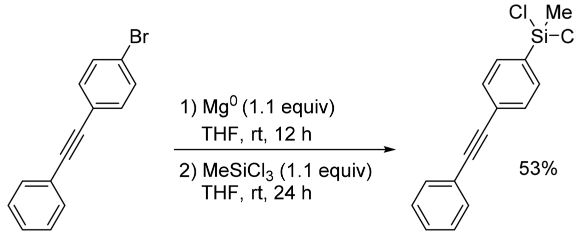

the Mg^0 turnings. This mixture was allowed to stir for 12 h after which a green solution was observed. An aliquot of the solution was dissolved in methanol, and GC/MS showed only one peak with an m/z of 178 suggesting full Grignard formation was achieved. In a 500 mL round-bottom flask equipped with a stir bar under an N_2 atmosphere, $MeSiCl_3$ (10 mL, 0.085 mol, 1.1 equiv) was placed in 40 mL of THF. The $MeSiCl_3$ was freshly distilled over CaH_2. The Grignard solution was cannula transferred dropwise into the 500 mL flask containing $MeSiCl_3$. The cannula transfer took approximately 45 min. The reaction mixture was allowed to stir for 24 h at which time GC–MS showed full conversion. It should be noted that the initial color of the solution was clear colorless, which turned first yellow, then green, and finally a yellow-orange color. At the end of the reaction, the excess THF and $MeSiCl_3$ were removed leaving behind a yellow powder. Fresh hexanes (~300 mL) were added to the powder creating a slurry. This slurry was filtered through a medium fritted funnel with the use of hexanes (~200 mL) to aid transfer and wash the solid on the frit. The solvent from the filtrate was removed producing a yellow solid which was dried under vacuum overnight at room temperature. Once dry, the solid was subjected to sublimation at 70 °C under 0.01 Torr. It should be noted that after the first batch a crystalline product was collected and the temperature of the sublimation was raised to 95 °C. Dichloro(methyl)(4-(phenylethynyl)phenyl)silane was collected as white crystals (12.1 g, 53% yield) with a melting point of 78 °C. ^{1}H NMR (500 MHz, $CDCl_3$) δ 7.71 (d, J = 8.2 Hz, 2H), 7.65–7.58 (m, 2H), 7.58–7.53 (m, 2H), 7.37 (dd, J = 4.8, 1.9 Hz, 3H), 1.05 (s, 3H). ^{13}C NMR (126 MHz, $CDCl_3$) δ 133.20, 132.98, 131.75, 131.24, 128.70, 128.43, 126.72, 122.78, 91.64, 88.69, 5.52. ^{29}Si NMR (99 MHz, $CDCl_3$) δ 18.39.

Capping of DDSQ-(Ph)$_8$(OH)$_4$. DDSQ-2((Me)(R)) compounds, where R = *para*-phenylamine (PA) **2**, *para*-(phenylethynyl)phenyl (PEP) **3**, and phenyl (Ph) **4**, were synthesized following Scheme 1 and are shown in Figure 2. A 250 mL flask was charged with DDSQ-(Ph)$_8$(OH)$_4$ (**1**) (2.0 g, 1.87 mmol, 1 equiv) and a stir bar and then purged with dry N_2 for 15 min followed by the addition of THF (60 mL) at room temperature. To the solution was added $Cl_2Si(Me)(R)$ (3.74 mmol, 2 equiv) followed by dropwise addition of Et_3N (1.04 mL, 7.48 mmol, 4 equiv). The addition of triethylamine took 5 min in total, and a cloudy white suspension was formed. The reaction mixture was stirred for 4 h. The solution was then filtered through a fine fritted funnel filter to remove the solid triethylamine hydrochloride. The solution was dried by rotary evaporation to afford *cis*-to-*trans* mixtures of DDSQ-2((Me)(R)) as a white powder. Compound **2** was obtained after deprotection of the trimethylsilyl groups using previously reported methods of methanol acidified with acetic acid and further evaporation of the volatiles.[58,62]

These reactions generated two geometrical arrangements for Me and R. When both moieties are facing in the same directions, they are referred to as *cis* isomers, and when they are facing in opposite directions, they are identified as *trans* isomers. The structures synthesized under this procedure are listed in Figure 2.

Analytical Methods. ^{1}H, ^{13}C, and ^{29}Si NMR spectroscopies were used to identify synthesized products. The *cis*-to-*trans* ratio of all samples investigated was first estimated using ^{29}Si NMR. Detailed quantification for the *cis*-to-*trans* ratio in **2** was performed based on ^{1}H NMR using a 2D NMR technique previously described.[58]

In general, separation of isomers was by fractional crystallization (FC) with THF as a good solvent and hexanes as a poor solvent using a procedure specified elsewhere.[14] Several cycles of fractional crystallization were needed for required isomer purity. Isolated isomers were crystallized by slow evaporation of THF, and crystals obtained were mounted on a nylon loop with Paratone oil and analyzed on a Bruker APEX-II CCD diffractometer. The crystal was kept at a constant temperature of 173 K during data collection.

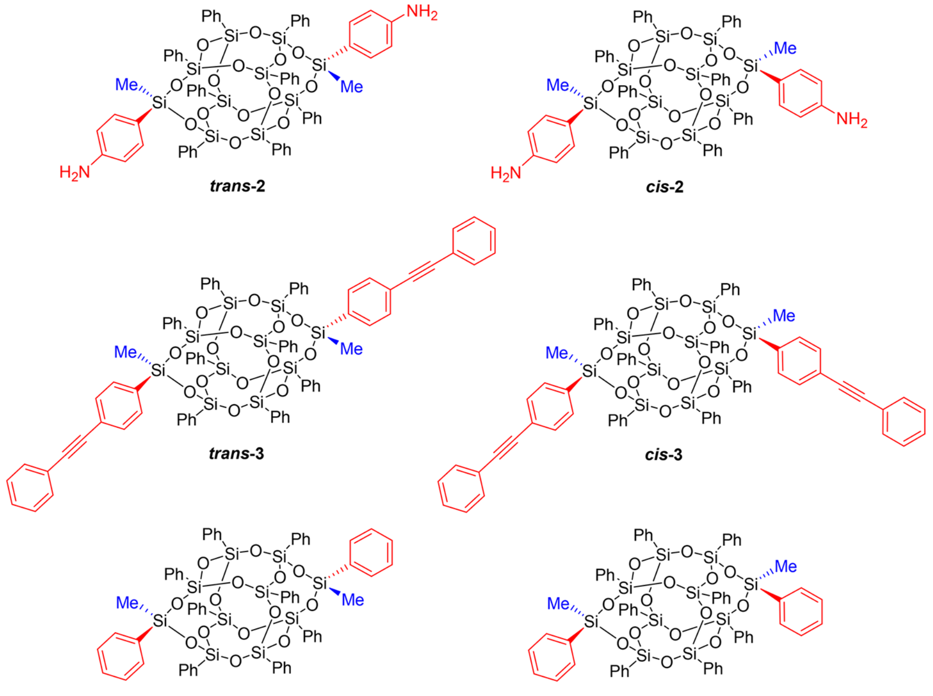

trans-2 *cis*-2

trans-3 *cis*-3

trans-4 *cis*-4

Figure 2. Structures synthesized and studied in this work.

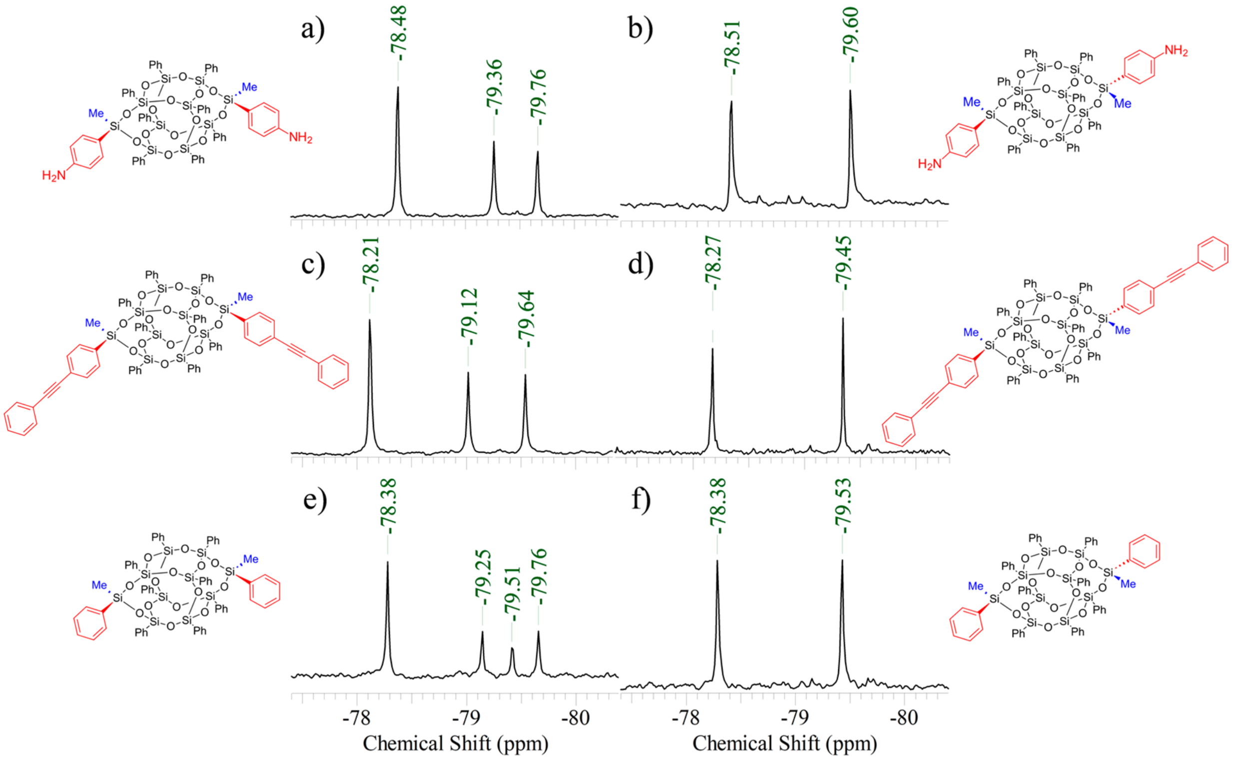

Figure 3. ^{29}Si NMR peaks representing the nearly pure isomers after separation: (a) *cis*-**2**, (b) *trans*-**2**, (c) *cis*-**3**, (d) *trans*-**3**, (e) 75% *cis*-**4**, (f) *trans*-**4**.

Table 1. Characteristics of Crystal Structures of Individual Isomers

compd	density (g/cm^3)	crystal system	space group	unit cell axes dimension (Å)		unit cell inclination angles (deg)	
cis-**2**	1.366	triclinic	$P\bar{1}$ (2)	*a*	13.77	*α*	87.11
				b	17.50	*β*	79.16
				c	27.50	*γ*	87.39
trans-**2**	1.390	monoclinic	$P2_1/n$ (14)	*a*	10.05	*α*	90.00
				b	43.57	*β*	91.66
				c	14.59	*γ*	90.00
cis-**3**	1.321	triclinic	$P\bar{1}$ (2)	*a*	14.44	*α*	85.92
				b	14.90	*β*	74.70
				c	18.54	*γ*	79.89
trans-**3**	1.341	triclinic	$P\bar{1}$ (2)	*a*	10.77	*α*	91.39
				b	13.45	*β*	108.68
				c	13.61	*γ*	91.69
trans-**4**	1.382	triclinic	$P\bar{1}$(2)	*a*	9.90	*α*	65.65
				b	13.51	*β*	71.77
				c	14.03	*γ*	69.54

Thermal behavior of isomers with purities superior to 95%, or nearly pure isomers, and mixtures of *cis* and *trans* isomers was studied by DSC Q2000 equipped with a mechanical cooling accessory. Typically, the temperature range of investigation was from 50 to 350 °C with a constant heating rate of 10 °C/min.

■ RESULTS AND DISCUSSION

Separation and Identification of Nearly Pure Isomers. Nearly pure *trans* and enriched *cis* DDSQ-2((Me)(R)) isomers can be obtained by fractional crystallization;[62] however, the ease of isolating nearly pure *cis* or *trans* isomers varied depending on the R group. In general, the as-synthesized DDSQ-2((Me)(R)) mixtures were dissolved in THF, and addition of hexanes resulted in crystallization and precipitation of the *trans* isomers. This in turn enriched the solution with the *cis* isomer. The isolation process was repeated until sufficiently isomerically pure compounds were obtained. Isolation of nearly pure *cis* and *trans* isomers by FC was easily achieved for **3**. However, separation of the *cis and trans* isomers of **4** required multiple recrystallizations. The nearly pure *trans*-**4** was obtained in the first cycle with this technique, but further removal of *trans* from the mother liquor could not be achieved after a threshold of 75 wt % *cis* and 25 wt % *trans* was reached. Unfortunately, further purification via LC was unable to increase the *cis* isomer ratio due to nonpolar R groups in **4**.[60,66] The *trans* isomers were isolated by FC for **2**. Due to the polar nature of phenylamines in **2**, liquid chromatography proved effective for the isolation of nearly pure *cis* fraction.[10,14] The isolated isomers were analyzed by ^{29}Si NMR, as seen in Figure

3. Analysis by HPLC can be observed in the Supporting Information file.

Isolated isomers were crystallized by slow evaporation of THF to form single crystals needed for crystallographic analysis. We obtained crystallographic data for each compound; however, it should be noted that *cis*/*trans*-**2** and *cis*/*trans*-**3** were previously reported.[64,67] Data from these crystal structures are shown in Table 1. Crystalline packing density for the *cis* isomer is less than for the *trans* isomer, and packing density was reduced as the size of R group in DDSQ-2((Me)(R)) increases.

Thermal Behavior of Nearly Pure Isomers. Melting behavior as expressed in DSC trace for pure compounds is usually observed as a single sharp endothermic peak in which the onset temperature (T_{onset}) is very similar to the peak temperature (T_{peak}). This was observed for *cis*-**2**, *trans*-**2**, and *trans*-**3** indicating the purity of these samples was >95% based on the difference between T_{onset} and T_{peak} and the ^{29}Si NMR spectra shown in Figure 3. However, for *cis*-**3** and *trans*-**4** approximately 6 °C difference in T_{onset} and T_{peak} was large enough to indicate these compounds may not be as pure as suggested by ^{29}Si NMR. In fact a first small endo peak with an onset temperature near 267 °C was observed for DSC trace of nearly pure *trans*-**4**. Melting temperatures (T_{m}) calculated from the T_{onset} in the endo peak were higher for *trans* isomers than for *cis* isomers as seen in Table 2. The calculated entropy at melting (ΔS_{m}) for *trans* isomers is higher than *cis* isomers. This suggests the solid state of the *trans* isomer is more ordered than that of the *cis* isomer. From Table 2, it was observed that the size of the R group could affect the value of T_{m}. Larger R has a lower value of T_{m}. The T_{m} reduction is most likely related to the packing density as reported in Table 1.

Table 2. Experimental Values Obtained from Nearly Pure *cis* and *trans* DDSQ-2((Me)(R)) by DSC[a]

compd	T_{peak} (°C)	T_{m} (°C)	ΔH_{m} (kJ/mol)	ΔS_{m} (J mol^{-1} K^{-1})
cis-2	277.9	275.7	37.8	69
trans-2	313.0	310.6	54.6	94
cis-3	269.9	263.1	46.7	87
trans-3	302.7	300.0	63.7	128
trans-4	320.8	313.9	58.9	99

[a] $\Delta S_{\text{m}} = \Delta H_{\text{m}}/T_{\text{m}}$.

Phase Behavior of *cis*–*trans* Binary Mixtures. Knowing that evaluated isomers have different crystal structures, we hypothesized that they may be immiscible in the solid state. Hence, it is possible for a mixture with a specified *cis*-to-*trans* ratio to exhibit eutectic transition. From the thermal analysis results for individual isomers, solid–liquid phase diagrams were calculated from the Schröder–van Laar equation (eq 1),[68] where x_i is the mole fraction of the isomer i in the mixture, $\Delta H_{\text{m}i}$ is the heat of fusion of the pure compound i, R is the gas constant, T is variable temperature, and $T_{\text{m}i}$ is the melting temperature of compound i. Ideal behavior in the phase equilibrium was assumed such that the activity coefficient (γ_i) value was set to 1. Mixtures with near-eutectic compositions based on the calculated phase diagrams were prepared from the previously isolated isomers.

$$\ln(x_i \gamma_i) = \frac{\Delta H_{\text{m}i}}{RT}\left(1 - \frac{T}{T_{\text{m}i}}\right) \tag{1}$$

Analysis of DSC curves for different *cis* to *trans* ratios was completed following the standard methodology used in the analysis of binary metallic alloys.[69] Here, the onset temperature of the lowest endo peak is denoted as the eutectic temperature (T_{E}), and the peak temperature of the highest endo peak is the liquidus temperature (T_{L}).

Solid–Liquid Phase Equilibrium of DDSQ-2((Me)(PA)) 2. Binary mixtures of **2** were prepared using the FC method by gradual removal of *trans* isomers and their compositions reported within were estimated by NMR. Most DSC traces of **2** have two endo peaks corresponding to eutectic and liquidus transition (Figure 4a). It was observed the value of T_{L} decreases as the amount of *cis* isomer increases in the mixture up to the eutectic composition. When x_{trans} in the mixture reaches a value of 0.33, only one peak was resolved. The onset temperature of this DSC trace is very similar to the onset of the first endo peak in DSC traces for up 0.7 of x_{trans} as shown in Figure 4a. This T_{onset} represents a near-eutectic composition. Below the eutectic point, where $x_{trans} = 0.20$, the melting endotherm appears to be very broad and is representative of two overlapping melting endotherms. This trace also shows some meta-eutectic behavior, which is why the first transition starts even lower than the eutectic. T_{onset} in the first endo peak agrees with the previously described eutectic temperature. For $x_{\text{trans}} = 0.50$ three endothermic transitions can be observed; it is hypothesized that cocrystal behavior was formed possibly by interactions between amine moieties. Experimental onset temperatures and liquidus temperatures were plotted, and a solid–liquid binary phase diagram of varying *cis*-to-*trans* ratios was constructed as shown in Figure 4b. The experimental results are relatively close to the ideal eutectic as described by eq 1.

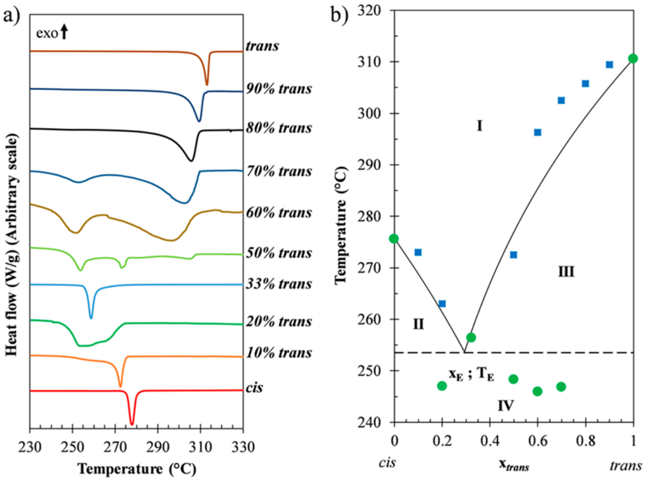

Figure 4. (a) DSC curves for compound **2**. Every curve was normalized for better identification of peaks. The reported x_{trans} was estimated using NMR. (b) Binary phase diagram for structure **2**. Green dots are the onset temperatures of the first endothermic transition in DSC trace. Blue squares represent the peak temperature of the highest endothermic transition. The solid line represents the ideal eutectic as calculated using eq 1. Dashed line represents the calculated eutectic temperature T_{E} which matches the transition temperature observed using a sample with the predicted eutectic composition. Phase I: $\text{L}_{(cis+trans)}$. Phase II: $\text{L}_{(cis+trans)} + \text{S}_{cis}$. Phase III: $\text{L}_{(cis+trans)} + \text{S}_{trans}$. Phase IV: $\text{S}_{cis} + \text{S}_{trans}$.

Solid–Liquid Phase Equilibrium of DDSQ-2((Me)(PEP)) 3. Phenylamine was replaced with a larger nonpolar

PEP group to reduce possible polar interactions. Nearly pure *cis*-**3** and nearly pure *trans*-**3** were separated and their purities analyzed by ^{29}Si NMR and HPLC using a Hypercarb column and ethyl acetate as the mobile phase. The nearly pure isomers were physically mixed, solubilized in THF, and dried using a dynamic vacuum. Three mixtures were prepared with x_{trans} = 0.3, 0.5, and 0.7. DSC traces for nearly pure isomers and their binary mixtures can be observed in Figure 5a. The trace for x_{trans} = 0.3 has a single relatively sharp peak. In contrast, traces for x_{trans} = 0.5 and 0.7 have two endo peaks. For these traces, T_{liquidus} decreased as the fraction of *cis* isomer increased in the sample. T_{onset} in the first endotherm transition for x_{trans} = 0.5 and 0.7 is similar to that of x_{trans} = 0.3. This result is distinguishing for eutectic temperature. T_{onset} of nearly pure *cis* is higher than T_{onset} of x_{trans} = 0.3 confirming the existence of a eutectic composition close to x_{trans} = 0.3. The calculated phase diagram is close to the collected data indicating proximity to ideal eutectic behavior for compound **3**. In Figure 5b are plotted the eutectic temperature and liquidus temperature for each mixture as well as the solid−liquid phase diagram. DSC traces for nearly pure *cis* and nearly pure *trans* in Figure 5a are similar to the same traces reported in a prior study.[64] However, the DSC trace for x_{trans} = 0.5 is inconsistent between this and work reported by Moore et al. as they overlooked the existence of the eutectic reaction.

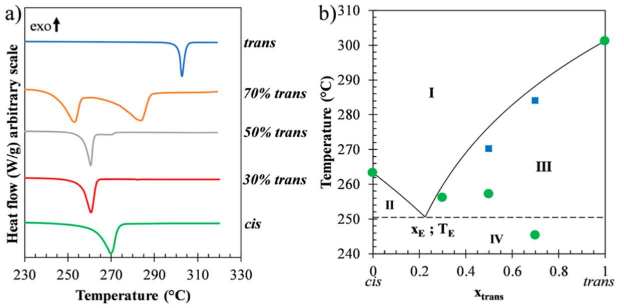

Figure 5. (a) DSC curves for compound **3**. Every curve was normalized for better identification of peaks. () Binary phase diagram for structure **3**. Green dots are the onset temperatures of the first endothermic transition in DSC trace. Blue squares represent the peak temperature of the highest endothermic transition. The solid line represents the ideal eutectic as calculated using eq 1. Dashed line represents the calculated eutectic temperature T_E. Phase I: $L_{(cis+trans)}$. Phase II: $L_{(cis+trans)}$ + S_{cis}. Phase III: $L_{(cis+trans)}$ + S_{trans}. Phase IV: S_{cis} + S_{trans}.

Solid−Liquid Phase Equilibrium of DDSQ-2((Me)(Ph)) 4. Structure **4** was analyzed to reveal the phase behavior of a DDSQ structure with the smallest aryl group possible. After synthesis of **4**, *trans* isomers were progressively removed by FC. DSC trace for x_{trans} = 0.33 resulted in a single peak. Two endotherms were identified in all others including nearly pure *trans*-**4**. T_{liquidus} steadily decreased as the fraction of *cis* isomer increased up to x_{trans} = 0.33. T_{onset} of the first endo peak has similar value as the T_{onset} for the single peak observed in x_{trans} = 0.33, which represents the eutectic temperature (Figure 6a). For x_{trans} = 0.25, its DSC trace has a main peak and a shoulder. The first main peak has a T_{onset} similar to the eutectic temperature. The shoulder located between 275 and 285 °C is the T_{liquidus} for the excess *cis* isomer-rich phase in the mixture. Pure *cis*-**4** was never isolated despite several crystallization attempts. It is believed that samples with compositions of *cis* isomers larger than 75% may be forming cocrystals, making further removal of *trans*-**4** very difficult. The phase diagram in Figure 6b is near the ideal for the hypereutectic *trans*-rich portion. The experimentally near-eutectic composition (x_{trans} = 0.33) is extracted by fitting with the calculated trace for *trans*-**4**. The eutectic composition cannot be calculated due to the lack of available nearly pure *cis*-**4**.

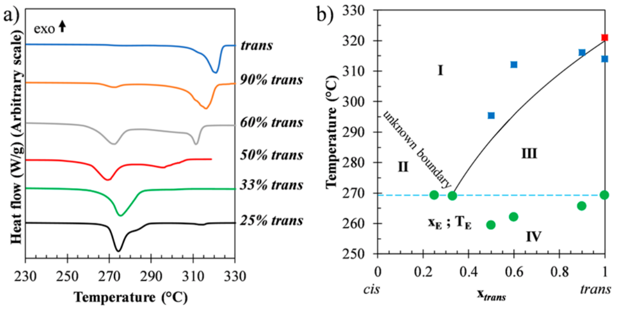

Figure 6. (a) DSC curves for compound **4**. Every curve was normalized for better identification of peaks. (b) Partial binary phase diagram for structure **4**. Green dots are the onset temperatures of the first endothermic transition in DSC trace. Blue squares represent the peak temperature of the highest endothermic transition. The solid line represents the ideal solid−liquid equilibrium. Light blue dashed line represents the experimental eutectic temperature T_E. For nearly pure *trans*-**4** are depicted the nearly eutectic temperature from the first endo peak (green dot), the onset temperature from the second endo peak (blue square), and the peak temperature from the second endo peak (red square). Phase I: $L_{(cis+trans)}$. Phase II: $L_{(cis+trans)}$ + S_{cis}. Phase III: $L_{(cis+trans)}$ + S_{trans}. Phase IV: S_{cis} + S_{trans}.

■ CONCLUSIONS

Eutectic temperatures were observed for the DDSQ-2((Me)(R)) mixtures studied in this work. The eutectic composition was generally located near x_{trans} = 0.3. Excitingly, the eutectic temperature was on average 50 °C lower than the melting temperature of nearly pure *trans* isomers. DSC traces for the composition obtained after reaction (x_{trans} = 0.5) have liquidus temperatures 20 °C larger than the temperatures in the eutectic composition. This result indicates that liquid processing of materials containing DDSQ-2((Me)(R)) is milder from a temperature perspective if a near-eutectic composition is used for such process. Onset temperature in the endothermic transition for nearly pure and for nearly eutectic composition is inversely proportional to the size of the R group. This result indicates that selection of high steric R groups will result in lower melting temperatures for the nearly pure isomers, as well as at the eutectic transition. These data allow users to tune the melting temperature of the materials either by adjusting the sterics in the system or by adjusting the ratio of *cis*-to-*trans* isomers.

■ ASSOCIATED CONTENT

Ⓢ Supporting Information

The Supporting Information is available free of charge on the ACS Publications website at DOI: 10.1021/acsanm.8b02114.

Spectral and crystallographic data of all synthesized materials and summarized eutectic and liquidus compositions (PDF)

AUTHOR INFORMATION

Corresponding Authors

*R.E.M.: e-mail, maleczka@chemistry.msu.edu; phone, (517) 353-0834.

*A.L.: e-mail, leea@egr.msu.edu; phone, (517) 355-5112.

ORCID

Robert E. Maleczka, Jr.: 0000-0002-1119-5160

Andre Lee: 0000-0001-6921-7214

Funding

This work was funded by the Office of Naval Research Grant N00014-16-2109.

Notes

The authors declare no competing financial interest.

ACKNOWLEDGMENTS

We thank program manager William Nickerson for his support.

REFERENCES

(1) Phillips, S. H.; Haddad, T. S.; Tomczak, S. J. Developments in Nanoscience: Polyhedral Oligomeric Silsesquioxane (POSS)-Polymers. *Curr. Opin. Solid State Mater. Sci.* **2004**, *8* (1), 21−29.

(2) Li, G.; Wang, L.; Ni, H.; Pittman, C. U. Polyhedral Oligomeric Silsesquioxane (POSS) Polymers and Copolymers: A Review. *J. Inorg. Organomet. Polym.* **2001**, *11* (3), 123−154.

(3) Feher, F. J.; Phillips, S. H.; Ziller, J. W. Facile and Remarkably Selective Substitution Reactions Involving Framework Silicon Atoms in Silsesquioxane Frameworks. *J. Am. Chem. Soc.* **1997**, *119* (14), 3397−3398.

(4) Feher, F. J.; Newman, D. A.; Walzer, J. F. Silsesquioxanes as Models for Silica Surfaces. *J. Am. Chem. Soc.* **1989**, *111* (5), 1741−1748.

(5) Feher, F. J.; Walzer, J. F. Synthesis and Characterization of Vanadium-Containing Silsesquioxanes. *Inorg. Chem.* **1991**, *30* (8), 1689−1694.

(6) Morimoto, Y.; Watanabe, K.; Ootake, N.; Inagaki, J.-I.; Yoshida, K.; Ohguma, K. Silsesquioxane Derivatives and Process for Production Thereof. U.S. Patent US20040249103A1, December 9, 2004.

(7) Lee, D. W.; Kawakami, Y. Incompletely Condensed Silsesquioxanes: Formation and Reactivity. *Polym. J.* **2007**, *39* (3), 230−238.

(8) Hoque, M. A.; Kakihana, Y.; Shinke, S.; Kawakami, Y. Polysiloxanes with Periodically Distributed Isomeric Double-Decker Silsesquioxane in the Main Chain. *Macromolecules* **2009**, *42* (9), 3309−3315.

(9) Kawabata, K.; Tajima, A.; Matsuo, T.; Watanabe, Y.; Ayama, K. Compound Including Organopolysiloxane or Silsesquioxane Skeleton Having Isocyanuric Skeleton, Epoxy Group and SiH Group, Thermosetting Resin Composition Containing the Compound as Adhesion-Imparting Agent, Hardened Material and Sealing Agent for Optical Semiconductor. U.S. Patent 20140148536A1, May 29, 2014.

(10) Au-Yeung, H.-L.; Leung, S. Y.-L.; Yam, V. W.-W. Supramolecular Assemblies of Dinuclear Alkynylplatinum(II) Terpyridine Complexes with Double-Decker Silsesquioxane Nano-Cores: The Role of Isomerism in Constructing Nano-Structures. *Chem. Commun.* **2018**, *54* (33), 4128−4131.

(11) Wu, S.; Hayakawa, T.; Kakimoto, M.-A.; Oikawa, H. Synthesis and Characterization of Organosoluble Aromatic Polyimides Containing POSS in Main Chain Derived from Double-Decker-Shaped Silsesquioxane. *Macromolecules* **2008**, *41* (10), 3481−3487.

(12) Kucuk, A. C.; Matsui, J.; Miyashita, T. Langmuir-Blodgett Films Composed of Amphiphilic Double-Decker Shaped Polyhedral Oligomeric Silsesquioxanes. *J. Colloid Interface Sci.* **2011**, *355* (1), 106−114.

(13) Wu, S.; Hayakawa, T.; Kikuchi, R.; Grunzinger, S. J.; Kakimoto, M.-A.; Oikawa, H. Synthesis and Characterization of Semiaromatic Polyimides Containing POSS in Main Chain Derived from Double-Decker-Shaped Silsesquioxane. *Macromolecules* **2007**, *40* (16), 5698−5705.

(14) Jiang, Q.; Zhang, W.; Hao, J.; Wei, Y.; Mu, J.; Jiang, Z. A Unique "cage−cage" Shaped Hydrophobic Fluoropolymer Film Derived from a Novel Double-Decker Structural POSS with a Low Dielectric Constant. *J. Mater. Chem. C* **2015**, *3* (44), 11729−11734.

(15) Liu, N.; Li, L.; Wang, L.; Zheng, S. Organic-Inorganic Polybenzoxazine Copolymers with Double Decker Silsesquioxanes in the Main Chains: Synthesis and Thermally Activated Ring-Opening Polymerization Behavior. *Polymer* **2017**, *109* (Suppl. C), 254−265.

(16) Hoque, M. A.; Kawakami, Y. Synthesis of Polysilsesquioxanes with Double-Decker Silsesquioxane Repeating Units. *J. Sci. Res.* **2016**, *8* (2), 217−227.

(17) Żak, P.; Majchrzak, M.; Wilkowski, G.; Dudziec, B.; Dutkiewicz, M.; Marciniec, B. Synthesis and Characterization of Functionalized Molecular and Macromolecular Double-Decker Silsesquioxane Systems. *RSC Adv.* **2016**, *6* (12), 10054−10063.

(18) Haddad, T. S.; Viers, B. D.; Phillips, S. H. Polyhedral Oligomeric Silsesquioxane (POSS)-Styrene Macromers. *J. Inorg. Organomet. Polym.* **2001**, *11* (3), 155−164.

(19) Leu, C.-M.; Chang, Y.-T.; Wei, K.-H. Polyimide-Side-Chain Tethered Polyhedral Oligomeric Silsesquioxane Nanocomposites for Low-Dielectric Film Applications. *Chem. Mater.* **2003**, *15* (19), 3721−3727.

(20) Lichtenhan, J. D.; Schwab, J. J.; An, Y.; Liu, Q.; Haddad, T. S. Process for the Functionalization of Polyhedral Oligomeric Silsesquioxanes. U.S. Patent 6927270, August 9, 2005.

(21) Li, Y.; Dong, X.-H.; Zou, Y.; Wang, Z.; Yue, K.; Huang, M.; Liu, H.; Feng, X.; Lin, Z.; Zhang, W.; et al. Polyhedral Oligomeric Silsesquioxane Meets "click" Chemistry: Rational Design and Facile Preparation of Functional Hybrid Materials. *Polymer* **2017**, *125*, 303−329.

(22) Cao, J.; Fan, H.; Li, B.-G.; Zhu, S. Synthesis and Evaluation of Double-Decker Silsesquioxanes as Modifying Agent for Epoxy Resin. *Polymer* **2017**, *124*, 157−167.

(23) Xu, S.; Zhao, B.; Wei, K.; Zheng, S. Organic-Inorganic Polyurethanes with Double Decker Silsesquioxanes in the Main Chains: Morphologies, Surface Hydrophobicity, and Shape Memory Properties. *J. Polym. Sci., Part B: Polym. Phys.* **2018**, *56* (12), 893−906.

(24) Haddad, T. S.; Mabry, J. M.; Ramirez, S. Synthesis of Functional Fluorinated Polyhedral Oligomeric Silsesquioxane (F-POSS). U.S. Patent 9249313, February 2, 2016.

(25) Lee, A.; Lu, Y.; Roche, A.; Pan, T.-Y. Influence of Nano-Structured Silanols on the Microstructure and Mechanical Properties of A4047 and A359 Aluminum Casting Alloys. *Int. J. Metalcast.* **2016**, *10* (3), 338−341.

(26) Blanco, I.; Abate, L.; Bottino, F. A.; Bottino, P. Thermal Degradation of Hepta Cyclopentyl, Mono Phenyl-Polyhedral Oligomeric Silsesquioxane (hcp-POSS)/polystyrene (PS) Nanocomposites. *Polym. Degrad. Stab.* **2012**, *97* (6), 849−855.

(27) Jin, L.; Ishida, H. New Thermo-Oxidative Protective Coating for Carbon/carbon Composites in Mid-Temperature Range Using a Combination of Nano-Filler and Macro-Filler with Polybenzoxazine as a Carbon-Forming Matrix. *Polym. Compos.* **2011**, *32* (8), 1164−1173.

(28) Vahabi, H.; Eterradossi, O.; Ferry, L.; Longuet, C.; Sonnier, R.; Lopez-Cuesta, J.-M. Polycarbonate Nanocomposite with Improved Fire Behavior, Physical and Psychophysical Transparency. *Eur. Polym. J.* **2013**, *49* (2), 319−327.

(29) Ke, F.; Zhang, C.; Guang, S.; Xu, H. POSS Core Star-Shape Molecular Hybrid Materials: Effect of the Chain Length and POSS Content on Dielectric Properties. *J. Appl. Polym. Sci.* **2013**, *127* (4), 2628−2634.

(30) Ramirez, N. V.; Sanchez-Soto, M. Effects of POSS Nanoparticles on ABS-G-Ma Thermo Oxidation Resistance. *Polym. Compos.* **2012**, *33* (10), 1707−1718.

(31) Wang, Z.; Yonggang, L.; Huijuan, M.; Wenpeng, S.; Tao, L.; Cuifen, L.; Junqi, N.; Guichun, Y.; Zuxing, C. Novel Phosphorus-Nitrogen-Silicon Copolymers with Double-Decker Silsesquioxane in

the Main Chain and Their Flame Retardancy Application in PC/ABS. *Fire Mater.* **2018**, *42*, 946−957.

(32) Seurer, B.; Vij, V.; Haddad, T.; Mabry, J. M.; Lee, A. Thermal Transitions and Reaction Kinetics of Polyhederal Silsesquioxane Containing Phenylethynylphthalimides. *Macromolecules* **2010**, *43* (22), 9337−9347.

(33) Liu, N.; Wei, K.; Wang, L.; Zheng, S. Organic−inorganic Polyimides with Double Decker Silsesquioxane in the Main Chains. *Polym. Chem.* **2016**, *7* (5), 1158−1167.

(34) Cardiano, P.; Lazzara, G.; Manickam, S.; Mineo, P.; Milioto, S.; Lo Schiavo, S. POSS−Tetraalkylammonium Salts: A New Class of Ionic Liquids. *Eur. J. Inorg. Chem.* **2012**, *2012* (34), 5668−5676.

(35) Li, H.; Zhao, X.; Chu, G.; Zhang, S.; Yuan, X. One-Step Fabrication of a Superhydrophobic Polymer Surface from an Acrylic Copolymer Containing POSS by Spraying. *RSC Adv.* **2014**, *4* (107), 62694−62697.

(36) Xue, Y.; Wang, H.; Yu, D.; Feng, L.; Dai, L.; Wang, X.; Lin, T. Superhydrophobic Electrospun POSS-PMMA Copolymer Fibres with Highly Ordered Nanofibrillar and Surface Structures. *Chem. Commun.* **2009**, *42*, 6418−6420.

(37) Kucuk, A. C.; Matsui, J.; Miyashita, T. Synthesis and Photochemical Response of Ru(II)-Coordinated Double-Decker Silsesquioxane. *RSC Adv.* **2018**, *8* (4), 2148−2156.

(38) Espinas, J.; Pelletier, J. D. A.; Abou-Hamad, E.; Emsley, L.; Basset, J.-M. A Silica-Supported Double-Decker Silsesquioxane Provides a Second Skin for the Selective Generation of Bipodal Surface Organometallic Complexes. *Organometallics* **2012**, *31* (21), 7610−7617.

(39) Hartmann-Thompson, C. *Applications of Polyhedral Oligomeric Silsesquioxanes*; Springer Science & Business Media, 2011.

(40) He, F.-A.; Zhang, L.-M. Using Inorganic POSS-Modified Laponite Clay to Support a Nickel α-Diimine Catalyst for in Situ Formation of High Performance Polyethylene Nanocomposites. *Nanotechnology* **2006**, *17* (24), 5941.

(41) Tanaka, K.; Ishiguro, F.; Chujo, Y. POSS Ionic Liquid. *J. Am. Chem. Soc.* **2010**, *132* (50), 17649−17651.

(42) Tanaka, K.; Ishiguro, F.; Jeon, J.-H.; Hiraoka, T.; Chujo, Y. POSS Ionic Liquid Crystals. *NPG Asia Mater.* **2015**, *7*, e174.

(43) Tanaka, K.; Ishiguro, F.; Chujo, Y. Thermodynamic Study of POSS-Based Ionic Liquids with Various Numbers of Ion Pairs. *Polym. J.* **2011**, *43*, 708.

(44) Zhao, R.; Chen, Y.; Liu, G.; Jiang, Y.; Chen, K. Fabrication of Self-Healing Waterbased Superhydrophobic Coatings from POSS Modified Silica Nanoparticles. *Mater. Lett.* **2018**, *229*, 281−285.

(45) Rizvi, S. B.; Yildirimer, L.; Ghaderi, S.; Ramesh, B.; Seifalian, A. M.; Keshtgar, M. A Novel POSS-Coated Quantum Dot for Biological Application. *Int. J. Nanomed.* **2012**, *7*, 3915−3927.

(46) Ganesh, V. A.; Nair, A. S.; Raut, H. K.; Tan, T. T. Y.; He, C.; Ramakrishna, S.; Xu, J. Superhydrophobic Fluorinated POSS-PVDF-HFP Nanocomposite Coating on Glass by Electrospinning. *J. Mater. Chem.* **2012**, *22* (35), 18479−18485.

(47) Wang, D. K.; Varanasi, S.; Strounina, E.; Hill, D. J. T.; Symons, A. L.; Whittaker, A. K.; Rasoul, F. Synthesis and Characterization of a POSS-PEG Macromonomer and POSS-PEG-PLA Hydrogels for Periodontal Applications. *Biomacromolecules* **2014**, *15* (2), 666−679.

(48) Tanaka, K.; Ohashi, W.; Kitamura, N.; Chujo, Y. Reductive Glutathione-Responsive Molecular Release Using Water-Soluble POSS Network Polymers. *Bull. Chem. Soc. Jpn.* **2011**, *84* (6), 612−616.

(49) Kolel-Veetil, M. K.; Fears, K. P.; Qadri, S. B.; Klug, C. A.; Keller, T. M. Formation of a Crosslinked POSS Network by an Unusual Hydrosilylation: Thermo-Oxidative Stabilization of the α-Cristobalite Phase in Its Amorphous Regions. *J. Polym. Sci., Part A: Polym. Chem.* **2012**, *50* (15), 3158−3170.

(50) Bagheri, H.; Soofi, G.; Javanmardi, H.; Karimi, M. A 3D Nanoscale Polyhedral Oligomeric Silsesquioxanes Network for Microextraction of Polycyclic Aromatic Hydrocarbons. *Microchim. Acta* **2018**, *185* (9), 418.

(51) Ghanbari, H.; Cousins, B. G.; Seifalian, A. M. A Nanocage for Nanomedicine: Polyhedral Oligomeric Silsesquioxane (POSS). *Macromol. Rapid Commun.* **2011**, *32* (14), 1032−1046.

(52) Tan, A.; Farhatnia, Y.; Seifalian, A. M. Polyhedral Oligomeric Silsesquioxane Poly (carbonate-Urea) Urethane (POSS-PCU): Applications in Nanotechnology and Regenerative Medicine. *Crit. Rev. Biomed. Eng.* **2014**, *41* (6), 495−513.

(53) Olivero, F.; Renò, F.; Carniato, F.; Rizzi, M.; Cannas, M.; Marchese, L. A Novel Luminescent Bifunctional POSS as a Molecular Platform for Biomedical Applications. *Dalton Trans.* **2012**, *41* (25), 7467−7473.

(54) Pu, Y.; Zhang, L.; Zheng, H.; He, B.; Gu, Z. Drug Release of pH-Sensitive poly(L-Aspartate)-B-Poly(ethylene Glycol) Micelles with POSS Cores. *Polym. Chem.* **2014**, *5* (2), 463−470.

(55) Schoen, B. W. Aminophenyl Double Decker Silsesquioxanes: Spectroscopic Elucidation, Physical and Thermal Characterization, and Their Applications. Ph.D. Thesis, Michigan State University, East Lansing, MI, 2013.

(56) Guo, T.; Wang, B. Isothermal Cold Crystallization and Melting Behaviors of Poly(lactic acid)/Epoxy Vinyl Polyhedral Oligomeric Silsesquioxanes Nanocomposites. *Polym.-Plast. Technol. Eng.* **2014**, *53* (9), 917−926.

(57) Li, Y.; Morgan, R. J. Thermal Cure of Phenylethynyl-Terminated AFR-PEPA-4 Imide Oligomer and a Model Compound. *J. Appl. Polym. Sci.* **2006**, *101* (6), 4446−4453.

(58) Schoen, B. W.; Holmes, D.; Lee, A. Identification and Quantification of Cis and Trans Isomers in Aminophenyl Double-Decker Silsesquioxanes Using 1H–29Si gHMBC NMR. *Magn. Reson. Chem.* **2013**, *51* (8), 490−496.

(59) Walczak, M.; Januszewski, R.; Majchrzak, M.; Kubicki, M.; Dudziec, B.; Marciniec, B. Unusual Cis and Trans Architecture of Dihydrofunctional Double-Decker Shaped Silsesquioxane and Synthesis of Its Ethyl Bridged π-Conjugated Arene Derivatives. *New J. Chem.* **2017**, *41* (9), 3290−3296.

(60) Vogelsang, D. F.; Maleczka, R. E.; Lee, A. HPLC Characterization of Cis and Trans Mixtures of Double-Decker Shaped Silsesquioxanes. *Silicon* **2019**, *11*, 5−13.

(61) Attanayake, G. K. Study of Different Routes to Develop Asymmetric Double Decker Silsesquioxane (DDSQ). Master's Thesis, Michigan State University, East Lansing, MI, 2015.

(62) Schoen, B. W.; Lira, C. T.; Lee, A. Separation and Solubility of Cis and Trans Isomers in Nanostructured Double-Decker Silsequioxanes. *J. Chem. Eng. Data* **2014**, *59* (5), 1483−1493.

(63) Ervithayasuporn, V.; Sodkhomkhum, R.; Teerawatananond, T.; Phurat, C.; Phinyocheep, P.; Somsook, E.; Osotchan, T. Unprecedented Formation of Cis-and Trans-Di [(3-Chloropropyl) Isopropoxysilyl]-Bridged Double-Decker Octaphenylsilsesquioxanes. *Eur. J. Inorg. Chem.* **2013**, *2013* (19), 3292−3296.

(64) Moore, L. M. J.; Zavala, J. J.; Lamb, J. T.; Reams, J. T.; Yandek, G. R.; Guenthner, A. J.; Haddad, T. S.; Ghiassi, K. B. Bis-Phenylethynyl Polyhedral Oligomeric Silsesquioxanes: New High-Temperature, Processable Thermosetting Materials. *RSC Adv.* **2018**, *8* (48), 27400−27405.

(65) Thogiti, S.; Parvathaneni, S. P.; Keesara, S. Polymer Anchored 3-Benzoyl-1-(1-Benzylpiperidin-4-Yl)-2-Thiopseudourea-Pd(II) Complex: An Efficient Catalyst for the Copper and Solvent Free Sonogashira Cross-Coupling Reaction. *J. Organomet. Chem.* **2016**, *822*, 165−172.

(66) Vogelsang, D. F.; Dannatt, J. E.; Maleczka, R. E., Jr.; Lee, A. Separation of Asymmetrically Capped Double-Decker Silsesquioxanes Mixtures. *Polyhedron* **2018**, *155*, 189−193.

(67) Vij, V.; Haddad, T. S.; Yandek, G. R.; Ramirez, S. M.; Mabry, J. M. Synthesis of Aromatic Polyhedral Oligomeric SilSesquioxane (POSS) Dianilines for Use in High-Temperature Polyimides. *Silicon* **2012**, *4*, 267−280.

(68) van Laar, J. J. Die Schmelz- Oder Erstarrungskurven Bei Binären Systemen, Wenn Die Feste Phase Ein Gemisch (amorphe Feste Lösung Oder Mischkristalle) Der Beiden Komponenten Ist. *Z. Phys. Chem.* **1908**, *63U* (1), 216−253.

(69) Boettinger, W. J.; Kattner, U. R.; Moon, K.-W.; Perepezko, J. NIST Recommended Practice Guide: DTA and Heat-Flux DSC Measurements of Alloy Melting and Freezing. Special Publication 960-15; National Institute of Standards and Technology, 2006.